

Tuning the magnetic properties of multisegmented Ni/Cu electrodeposited nanowires with controllable Ni lengths

M Susano^{1,†}, M P Proenca^{1,2,†}, S Moraes¹, C T Sousa^{1*} and J P Araújo¹

¹ *IFIMUP and IN-Institute of Nanoscience and Nanotechnology and Dep. Física e Astronomia, Universidade do Porto, Rua do Campo Alegre 687, 4169-007 Porto, Portugal.*

² *ISOM -*

[†] These authors have contributed equally to this work and both should be considered as first authors.

*E-mail: celiasousa@fc.up.pt

Abstract

The fabrication of segmented Ni/Cu nanowires (NWs), with tunable structural and magnetic properties, is reported. A potentiostatic electrodeposition method with a single electrolytic bath has been used to fabricate multisegmented Ni/Cu NWs inside a highly hexagonally ordered anodic nanoporous alumina membrane, with diameters of 50 nm and Ni segment lengths (L_{Ni}) tuned from 10 nm up to 140 nm. The X-ray diffraction results evidenced a strong dependence of the Ni NWs crystallographic face-centered-cubic (fcc) texture along the [220] direction on the aspect ratio of the NWs. The magnetic behavior of the multisegmented Ni/Cu NW arrays, as a function of the magnetic field and temperature, is also studied and correlated with their structural and morphological properties. Micromagnetic simulations, together with the experimental results, showed a dominant antiferromagnetic coupling between Ni segments along the wire length for small low aspect-ratio magnetic segments. When increasing the Ni segments' length, the magnetic interactions between these along the wire became stronger, favouring a ferromagnetic coupling. The Curie temperature of the NWs was also found to strongly depend on the Ni magnetic segment length. Particularly the Curie temperature was found to be reduced 75 K for the 20 nm Ni segments, following the finite-size scaling relation with $\xi_0 = 8.1 \text{ \AA}$ and $\gamma = 0.48$. These results emphasize the advantages of using a template assisted method to electrodeposit multilayer NWs, as it allows an easy tailor of the respective morphological, chemical, structural and magnetic properties.

1. Introduction

The optimization and accurate understanding of the fabrication process of segmented nanowires (NWs) using nanoporous templates and low-cost electrochemical deposition techniques is a subject of relevant interest due to the promising and outstanding applications of such wires [1-6]. In particular, Ni/Cu segmented NWs grown in anodic aluminium oxide (AAO) templates have received considerable attention, since one can easily tune the diameter and pore packaging density of the AAO template [4], and control at the nanometric scale the length of each magnetic segment and non-magnetic spacing by the deposition conditions [7-16]. The complexity, functionality and therefore the range of potential applications of the fabricated segmented NWs can be significantly increased by understanding their structural and magnetic properties, which depend on the accurate control of the fabrication methods. The number of layers, the used materials and dimensions, and the overall structural and magnetic properties are precisely controlled through pore design and electrodeposition tailor. This ability to control the size and aspect ratio of ferromagnetic segments and non-magnetic spacings in multilayered NWs allows one to tune additional degrees of freedom that have not been widely explored so far.

From the processing point of view electrochemical deposition is one of the most favourable techniques for the template-assisted fabrication of NWs [7-16]. This method allows one to easily tune the crystallographic structure and metal alloy composition of the NWs, by simply changing depositions conditions (time, applied potential and electrolyte), thus conditioning the respective physical response [17, 18]. Despite the well documented electrodeposition of multilayered NWs using different electrolytes for the deposition of each segment [7, 9, 10], this is a laborious process, especially when growing a large amount of multilayers. The co-deposition method is thus an excellent alternative, as it uses a single electrolytic bath and each material layer is deposited by changing the electrodeposition potential [11]. In this work, we used an improved co-deposition approach to deposit Ni/Cu multilayered NWs, in which only one electrolyte is used and the deposited material, as well as the deposition rate, are controlled by the applied potential and composition of the electrolyte, enabling a fast and easy growth of multisegmented NWs with reduced dimensions (few nanometers).

Single component magnetic NWs with high aspect ratios exhibit a behavior dominated by strong shape anisotropy and hence magnetization easy axis lying along the longitudinal direction [19]. However, when decreasing the NWs length to a lower aspect ratio (with length/diameter lower than 1), as in our approach, a pronounced interplay between the several magnetic anisotropies appears, which can lead to changes in the orientation of the magnetic easy axis [11]. Particularly, multisegmented NWs with alternated magnetic/nonmagnetic layers

exhibit interlayer coupling between the magnetic segments [13]. The ability to control the layers thickness and thus the aspect ratio of the magnetic segments provides an additional degree of freedom with particular interest [7, 14, 15]. Since the coercivity and remanence are dependent on the Ni length, diameter, interwire distance and Cu thickness, they can be tuned by selecting the appropriate Ni/Cu segmented NW dimensions. Another crucial aspect concerning the magnetic properties of Ni/Cu segmented NWs is the strong dependence of the Curie temperature on the Ni segments' length, which can also be used to tailor their magnetic response [1,3,5,6,12,20].

In this work, we have successfully fabricated Ni/Cu NWs, with Ni segment lengths between 10 and 140 nm and Cu layer thicknesses of around 35 to 75 nm, by template assisted electrodeposition using AAO membranes. The obtained NWs were subjected to structural (by X-ray diffraction, XRD), morphological (by scanning electron microscopy, SEM) and magnetic (by vibrating sample magnetometry, VSM) studies. The crystallographic texture along the Ni face-centered cubic (fcc) $\langle 220 \rangle$ direction is found to increase with the Ni segment's length. The magnetic properties of multilayered NWs are also highly dependent on the aspect ratio of the magnetic segment. In particular, the coercivity, remanence and Curie temperature of the NWs decrease for smaller Ni segment lengths. Micromagnetic simulations were also performed to better understand the magnetic properties of multisegmented Ni/Cu NW arrays as a function of the Ni and Cu thicknesses. This work thus reports an important contribution in the field of dipolar interactions and antiferromagnetic coupling exhibited between the Ni segments along the wire length and between the Ni segments of neighbouring wires in Ni/Cu segmented NW arrays, analysed both experimentally and theoretically.

2. Experimental details

2.1. Nanoporous alumina membranes

AAO templates were prepared by a standard two-step anodization method [21] of high-purity (> 99.999%) Al foils. Prior to anodization, Al foils were cleaned by means of ultrasonication in acetone and ethanol, 5 min each. In order to obtain ordered hexagonal nanopore arrays, first anodizations were performed at a constant voltage of 40 V for 24 h, in a 0.3 M oxalic acid solution at a temperature between 2°C and 6°C, thus forming a pre-patterned hole structure at the Al surface. The alumina was then removed by chemical etching in an aqueous solution of 0.2 M H_2CrO_4 and 0.4 M H_3PO_4 at room temperature for 24 h. Second anodizations were carried out using the same conditions as the first ones, but for 40 h, thus producing AAO membranes with $\approx 80 \mu\text{m}$ in thickness, pore diameters of $d \approx 35 \pm 5 \text{ nm}$ and interpore distances of $D_{\text{int}} \approx 105 \pm 5 \text{ nm}$. After the anodization process, a circle with 1 cm in diameter was opened

on the template backside, by wet chemical etching of the Al substrate in a 0.2 M CuCl_2 and 4.1 M HCl aqueous solution, at room temperature, allowing the AAO membrane to be enclosed in the Al template. Subsequently, the samples were immersed for 2 h in 0.5 M H_3PO_4 at room temperature to remove the alumina barrier layer present at the bottom of the nanopores, also increasing the pore diameter to around 50 ± 10 nm. A continuous Au layer was then sputtered on the backside of the AAO membrane to provide a conductive metallic contact at the bottom of the pores that will serve as the working electrode for the subsequent electrodeposition process.

2.2. Nanowires deposition

Multisegmented Ni/Cu NWs were electrochemically grown from an aqueous solution of 0.5 M $\text{NiSO}_4 \cdot 6\text{H}_2\text{O}$, 0.005 M $\text{CuSO}_4 \cdot 5\text{H}_2\text{O}$ and 0.6 M H_3BO_3 , at room temperature. Electrodeposition processes were carried out in a three-electrode cell equipped with an Ag/AgCl reference electrode, a Pt mesh as a counter electrode and the gold-coated AAO membrane acting as the working electrode. The composition of each Ni/Cu segment was obtained by adjusting the deposition potential at -1 V, for Ni deposition, and -0.4 V, for Cu deposition. The duration of the potentiostatic deposition pulses was adjusted accordingly with the calibrated deposition rate at each potential (≈ 1.6 nm/s at -1 V for Ni, and ≈ 0.3 nm/s at -0.4 V for Cu), thus accurately controlling the length (L) of each segment. The complete sequence consists of 300 cycles wherein each cycle corresponds to one segment of Ni and Cu. To ensure a homogeneous deposition of Ni/Cu NWs, a longer electrodeposition of Cu (15 min at -0.4 V) was first performed, filling the bottom of the pores with Cu NWs of approximately 200 nm in length.

2.3. Nanowires characterization

The morphologies and segmented distribution of the produced NWs were observed by SEM (FEI Quanta 400FEG Field Emission). Prior to the cross-sectional SEM imaging, the filled templates were immersed for a few seconds in 10% HNO_3 to selectively etch the Cu segments, thus helping the visualization of the different layers. Note that due to the close atomic number of Ni and Cu, these elements exhibit a similar brightness/contrast in the SEM images. Therefore, we had to remove the Cu layers by selective chemical etching prior to SEM imaging, in order to accurately measure the length of each segment (bright regions corresponded to the Ni segments, and black regions corresponded to the absence of segments and thus to the length of the etched layers of Cu). XRD (X'Pert PRO diffractometer) in the θ -2 θ geometry with Cu $K\alpha$ line ($\lambda = 0.15406$ nm) was used to determine the crystallographic structure of the electrodeposited NWs. The magnetic behaviour of the multisegmented Ni/Cu NWs embedded in the AAO template arrays was studied by means of a commercial Oxford Instruments 1.2 T resistive VSM equipped with a furnace, as a function of temperature [M(T); from 300 K to 700

K, at 10 kOe] and applied magnetic field [M(H); from 10 kOe to -10 kOe at 300 K]. The magnetic hysteresis loops [M(H)] were measured with the field (H) applied along the parallel (H^{\parallel}) and perpendicular (H^{\perp}) directions with respect to the NWs longitudinal axis.

2.4 Micromagnetic simulations

The magnetization reversal mechanisms of different arrays of multisegmented Ni/Cu NWs were studied by micromagnetic simulations using the Object Oriented MicroMagnetic Framework (OOMMF) project [22]. Ordered hexagonal arrays of 7 NWs with 50 nm in diameter and 105 nm of center-to-center distance were simulated. Each NW consisted in 3 Ni segments separated by 2 non-magnetic (Cu) segments. Two sets of simulations were made with Ni and Cu segments' lengths of (a) 20 and 25 nm, respectively; and (b) 60 and 75 nm, respectively. The saturation magnetization value of Ni was set to 490×10^3 A/m and the stiffness constant to 9×10^{-12} J/m. A cubic mesh with unit cell size of $(5 \times 5 \times 5)$ nm³ and a damping factor of 0.015 were used. The stopping condition used in our simulations was $|dm/dt| = 1$ deg/ns. The magnetic field was applied from 10 to -10 kOe along the axis of the NWs (z-direction) and perpendicular to the nanowires' long axis (x-direction).

3. Results and discussion

3.1. Morphological characterization

The pulsed electrodeposition potential sequence employed for the syntheses of multisegmented Ni/Cu NWs is showed in Fig. 1. Since the difference of the reduction potentials of Cu (+0.14 V vs. Ag/AgCl) and Ni (-0.45 V vs. Ag/AgCl) are sufficiently large (> 0.4 V) and the concentration of the more noble material is very low ($[Cu^{2+}] \ll [Ni^{2+}]$), low contaminated multilayers of Ni/Cu NWs are expected [11, 24]. Chen *et al.* have shown that due to the low Cu^{2+} concentration, the Cu deposition is diffusion-limited over a wide potential range from -0.15 V to -0.7 V [11]. Therefore, for Ni deposition at more negative potentials (-1 V), the molar fraction of Cu should be lower than 10% and Ni-rich segments are achieved in the Ni/Cu multisegmented NWs.

The SEM images in Fig. 2 display selected cross-sectional views of the Ni/Cu NWs grown in the AAO membrane. The layered structure and the reproducibility of the layer thickness are clearly seen, where homogeneous Ni segments (brighter sections) alternated with removed Cu layers (darker sections) are presented in the images. The analysis of the Ni/Cu interface using

high-resolution transmission electron microscopy has been previously reported by Chen et al. [23], in which sharp interfaces have been observed.

The NWs have a diameter of $\approx 50 \pm 10$ nm, corresponding to the respective pore size of the used AAO template. Ni segments' lengths (L_{Ni}) from 10 ± 5 nm up to 140 ± 8 nm were obtained (Fig. 2). Although the Cu electrodeposition parameters were maintained constant in all samples, for samples with low Ni lengths ($L_{Ni} < 30$ nm) the Cu segments' lengths (L_{Cu}) presented an average of 25 ± 5 nm, whereas the samples with $L_{Ni} > 60$ nm showed $L_{Cu} = 75 \pm 10$ nm. This can be attributed to the diffusion limited process in the small segments due to the very short deposition pulses [25-27].

3.2. Crystallographic structure

The crystallographic structure of the aligned Ni/Cu NWs embedded in the AAO template was analysed by measuring XRD scans, as shown in Fig. 3. The small peaks observed at 43.3° , 50.4° and 74.1° (Fig. 3.a) correspond to the electrodeposited Cu NWs [28]. The peaks presented at 38.2° , 44.4° , 64.8° and 77.5° can be ascribed to the Au layer sputtered at the bottom of the membranes. For Ni segments, a preferential face-centred cubic (fcc) structure was found, exhibiting three peaks at 44.5° , 51.8° and 76.4° that corresponded to the (111), (200) and (220) crystallographic planes, respectively (Fig. 3.a). Consequently, no oxide phase can be identified in these as-obtained NWs. Note, however, that the Ni (111) reflection is almost coincident with the Au (200). This was taken into account when analysing the Ni (111) peak intensity, assuming that a polycrystalline Au film was deposited. As the change in each peak's intensity is directly related to the amount of material deposited, we have analysed in Fig. 3.b the ratio between the intensities of Ni (220) and Ni (111) reflections. For Ni/Cu NWs with $L_{Ni} \geq 60$ nm, Ni with a crystallographic fcc structure strongly textured along the $\langle 220 \rangle$ direction is identified (Fig. 3.b), as previously reported for high aspect ratio NWs with similar dimensions deposited using template-assisted methods [29-31]. The XRD patterns of Ni/Cu NW arrays with $L_{Ni} = 20$ nm also illustrated a Ni fcc lattice, but this time with the $\langle 111 \rangle$ preferred direction. We find that the increase of Ni segments' length helps to improve the intensity and orientation of the Ni (220) peak (Fig. 3.b). This can be attributed to the growth of Ni segments with a highly oriented structure, in which $\langle 220 \rangle$ crystal axes align preferentially along the longitudinal axis of the NWs. This has been shown to strongly depend on the aspect ratio of the NWs, which in this case is given by the length of the Ni segments, and the geometrical confinement of the AAO template [27]. Besides, there is also an accompanying Cu diffraction with the same (220) orientation, showing that Cu segments tend to grow with the same crystalline orientation as the Ni segments in the Ni/Cu lattice NWs [16].

3.3. Magnetic properties

The magnetic properties of Ni/Cu multisegmented NWs embedded in the AAO membrane were studied by VSM. Figure 4 shows the magnetic hysteresis loops [$M(H)$] recorded for the Ni/Cu NWs with $L_{\text{Ni}} = 10$ nm (Fig. 4.a) and $L_{\text{Ni}} = 100$ nm (Fig. 4.b), with the applied magnetic field parallel (\parallel) and perpendicular (\perp) to the NWs long axis. The results illustrate a magnetic anisotropic behaviour for Ni/Cu NWs with the easy magnetization axis lying parallel to the wire axis [32], arising from the competition between the magnetocrystalline anisotropy and the shape anisotropy factors [33]. For the NWs with the smallest Ni segments' length (10 nm; Fig. 4.a) the parallel and perpendicular magnetic loops are very similar, exhibiting the lowest values of coercivity ($H_c^{\parallel} = 197 \pm 6$ Oe, $H_c^{\perp} = 118 \pm 17$ Oe) and normalized remanence ($m_r = M_r/M_{\text{Sat}}$, where M_r is the remanence and M_{Sat} is the saturation magnetization; $m_r^{\parallel} = 0.27 \pm 0.03$, $m_r^{\perp} = 0.1$).

Previous reports have shown that magnetic NWs with aspect ratios lower than 1 have an easy magnetization axis lying along the perpendicular direction [11, 34]. However, our results evidence the existence of an easy magnetization axis along the parallel direction for all samples, even for those with the smallest aspect ratios (of around 0.25). This behaviour may arise from the higher dipolar interactions exhibited between the Ni segments along the wire length than with Ni segments of neighbouring wires. In addition, for samples with $L_{\text{Ni}} \leq 30$ nm, the L_{Cu} was found to be around 25 nm and so the dipolar interactions between Ni segments of the same wire prevail, tilting the easy magnetization axis along the parallel direction [35, 36]. In order to better compare the dipolar interactions and antiferromagnetic coupling exhibited between the Ni segments along the wire length with those exhibited between the Ni segments of neighboring wires, micromagnetic simulations of selected arrays were performed using OOMMF. Figure 5 shows the simulated magnetic hysteresis loops obtained for $L_{\text{Ni}} = 20$ nm and $L_{\text{Cu}} = 25$ nm when applying the magnetic field both parallel and perpendicular to the multisegmented wire axis. For such small aspect ratio magnetic segments, the coercivities and remanence values obtained are very low and similar along both directions. Figure 5 also illustrates the cross-sections of the NW arrays at saturation ($H = 10$ kOe) and remanence ($H = 0$). Due to the small Cu (non-magnetic) spacing between the Ni layers and the low aspect ratio of the magnetic segments, an antiferromagnetic coupling between the Ni layers (when removing the applied magnetic field) is observed, both between the Ni segments along the wire length and with Ni segments of neighboring wires, for both directions of applied magnetic field. Also, the presence of small percentages of Cu in the Ni segments have already been reported to highly influence the

respective magnetic properties [34]. Since these chemical defects (higher Cu%) are expected to be mainly present at the extremities of the Ni segments (due to the co-deposition process used), for very small lengths, these will dominate the entire Ni sections, thus highly affecting their magnetic properties.

When increasing the Ni segments' length, much higher coercivity and normalized remanent magnetization values are observed along the parallel direction when compared to the perpendicular one. In particular, for NWs with $L_{\text{Ni}} = 100$ nm (Fig. 4.b), both the coercivity and remanence along the parallel direction are found to be around 5 times higher than along the perpendicular one ($H_c^{\parallel} = 757 \pm 10$ Oe, $H_c^{\perp} = 164 \pm 13$ Oe; $m_r^{\parallel} = 0.81 \pm 0.09$, $m_r^{\perp} = 0.10 \pm 0.02$). Figure 6 shows the simulated magnetic hysteresis loops of an array of Ni/Cu NWs with $L_{\text{Ni}} = 60$ nm and $L_{\text{Cu}} = 75$ nm, obtained when applying the magnetic field along both parallel (z-axis) and perpendicular (x-axis) directions. The simulated $M(H)$ loops illustrate the shape anisotropy effect of the higher aspect ratio NWs, in which higher coercivities and remanence values are obtained with the applied magnetic field along the NWs' long axis. When increasing the aspect ratio of the Ni segments, the interactions between the magnetic layers along the wire length are stronger, favouring a head-to-tail alignment (instead of an antiferromagnetic coupling) between the segments of each wire. Nevertheless, as the space between adjacent wires is kept the same, an antiferromagnetic coupling is still observed between the Ni segments of neighbouring wires, as illustrated in the cross-sections of the simulated NWs depicted in Figure 6 at $H_z = -400$ Oe, $H_x = 0$ and $H_x = -400$ Oe.

Figures 4.c and 4.d summarize the results obtained for the coercivities and normalized remanent magnetization values, respectively, for all the Ni/Cu NW samples and the two field orientations studied. As expected, both the coercivity and the remanence along the parallel direction increase with the aspect ratio of the Ni segments, illustrating their higher values for the sample with bigger L_{Ni} . On the other hand, along the perpendicular direction, these values are practically unaffected by the Ni segments length, since their diameter and center-to-center distance are kept constant.

The magnetic properties of the Ni/Cu NW arrays were also studied as a function of temperature (T). The $M(T)$ measurements were made under a constant applied magnetic field of 10 kOe from $T = 300$ to 700 K. The external magnetic field was applied parallel to the wire axis. In this temperature range, the Ni segments are expected to undergo a transition from ferromagnetic to paramagnetic, occurring at the so-called Curie temperature T_C ($T_C = 631$ K for bulk Ni) [12]. The Curie temperature is a critical point where a material's intrinsic magnetic moments change direction, and the material's magnetism goes from permanent (oriented magnetic moments) to induced (disordered behaviour). Figure 7.a shows a typical $M(T)$ measurement obtained for the Ni/Cu NWs with the biggest and the smallest (100 and 20 nm) Ni segments' length, where a

transition between two different regimes (with higher and lower magnetization values) are easily seen. This transition occurs at T_C , and can thus be estimated by the derivative of $M(T)$ (see inset in Fig. 7.a). Notice that, with the decrease of the Ni length, a broad transition is observed, which was ascribed to the increased size distribution of the Ni segments and also to the influence of the Cu contamination.

Figure 7.b displays the T_C values obtained as a function of the Ni segments' length. For Ni/Cu NWs, T_C is found to strongly depend on the length of the Ni magnetic segments, increasing with L_{Ni} . A shift of 75 K was measured for the 20 nm length Ni segments. The decrease of the Curie temperature with reducing length can be described by the finite-size scaling relation, as performed by several authors studying NWs with different dimensions [1,3,5,6,12, 20]. Bulk magnetic materials at temperatures close to the $T_c(\infty)$ exhibit an asymptotic behaviour described by a correlation length $\xi(T)$ of:

$$\xi(T) = \xi_0 \left| 1 - \frac{T}{T_c(\infty)} \right|^{-\nu} \quad (1)$$

where ξ_0 is the correlation length extrapolated for $T = 0$, which is a microscopic length close to the lattice constant, and ν is the critical exponent for correlation [37]. For magnetic NWs with length L , the growth of $\xi(T)$ is limited by the wire length, reducing the Curie temperature by:

$$T_C(L) = T_c(\infty) \left[1 - \left(\frac{\xi_0}{L} \right)^\gamma \right] \quad (2)$$

where $T_C(L)$ is the Curie temperature for NWs with length L , and $\gamma = 1/\nu$ is the shift exponent [12, 37].

Figure 8 shows a log-log plot of the Ni/Cu NWs Curie temperature $[T_c(\infty) - T_C(L)]/T_c(\infty)$ normalized to the Curie temperature for bulk Ni [$T_c(\infty) = 631$ K] versus Ni segment length, L . From the linear fit of the data represented in Fig. 8, we obtain $\gamma = 0.48$ and $\xi_0 = 8.1$ Å. The equation (1) is valid only for T_c closed to the bulk T_c , thus only applicable for system with relatively large dimensions (length and diameter). Therefore, for the low aspect-ratio Ni segments, the extrapolated correlation length, ξ_0 , presents a larger uncertainty. Even so, the obtained ξ_0 of 8.1 Å, is close to values of about 10 Å reported for epitaxial Ni thin films [38, 39] and for high aspect-ratio Ni NWs [12, 37]. On the other hand, the γ is lower than the theoretical values predicted by the 3D Heisenberg model ($\gamma = 1.4$) and the 3D Ising model ($\gamma = 1.58$) [9]. However, both models only consider nearest neighbours interactions, whereas Ni is a ferromagnet with long range interactions [12, 40]. There are many other models that can be used to interpret decrease of the Curie temperature with reducing length [41-43]. Nevertheless, the finite-size scaling model is the most reported model in the literature, was demonstrated to be in good agreement with other models [44, 45], and fits well our results.

Finally, when reducing the size of the Ni segments, the fluctuations of electron spins become more prominent thus decreasing the Curie temperature. The size of a particle also affects the

magnetic anisotropy causing the spins' alignment to become less stable and thus leading to disordered magnetic moments [46, 47]. In addition, the Curie temperature of nanoparticles is also affected by the crystal lattice structure as the magnetic moments react with their neighbouring electron spins. Here we have shown that the increase in L_{Ni} leads to a change of crystallographic orientation towards the Ni fcc (220) direction, where the structure is tighter and thus higher T_{C} values are also expected [47].

4. Conclusions

Ni/Cu multisegmented NW arrays, with around 50 nm in diameter and made of alternating segments respective of Ni and Cu, having Ni length from 10 nm up to 140 nm have been synthesized by template assisted electrochemical deposition into the pores of AAO templates by alternately varying between two different deposition potentials. NWs growth rate vary quasi-linearly with the deposition time. XRD results indicate that Ni/Cu segments present a fcc structure, whose texture strongly depends on the aspect ratio of the NWs. Magnetic measurements, as a function of the applied field and temperature, illustrated an increase in the coercivity, remanence and Curie temperature with the Ni segments' length, when applying the magnetic field along the parallel direction. Micromagnetic simulations illustrated the importance of the Ni and Cu segments' lengths on the tuning of the magnetic properties of the arrays. In particular, an antiferromagnetic coupling has been observed between the small aspect-ratio Ni segments along the wire length, while larger dipolar interactions between higher aspect-ratio Ni segments induced a ferromagnetic coupling along the wires. Also, the Curie temperature of Ni/Cu segmented NWs was found to decrease with the Ni NWs length following a finite-size scaling relationship. These results show that the magnetic properties of Ni/Cu NWs, such as the magnetic easy axis, dipolar interactions, coercivity, remanence and Curie temperature, can be tailored by engineering the magnetic/non-magnetic segmented NWs with different aspect ratios, diameters and non-magnetic interlayer thicknesses.

Acknowledgments

MPP and CTS acknowledge FCT for grants SFRH/BPD/84948/2012 and SFRH/BPD/82010/2011, respectively, supported by funding POPH/FSE. SM acknowledge to the Brazilian agencies CNPq, CAPES and FAPERJ for grant 234513/2014-4 C. The authors acknowledge funding from FCT through the Associated Laboratory IN and project UID/NAN/50024/2013, and from FEDER and ON2 through project Norte-070124-FEDER-000070.

References

1. Li F, Wang W, Li L, Zhang X, Wang J, Magnetic anisotropy and one-dimensionality finite-size scaling law in polycrystalline Ni nanowire arrays 2015 *J. Alloy. Compd.* 635, 21
2. Xiaoming K, Xin F, Randy K D, Qi L, Yaping Z, Zhu H, Zhang X, Liu K, and Xiao J Q, Memory Effect in Magnetic Nanowire Arrays 2011 *Adv. Mater.* 23 1393
3. Wang J, Wu W, Zhao F, Zhao GM, Finite-size scaling behavior and intrinsic critical exponents of nickel: Comparison with the three-dimensional Heisenberg model 2011 *Phys. Rev. B* 84, 174440
4. Sousa C T, Leitao D C, Proenca M P, Pereira A M, Ventura J, and Araujo J P Nanoporous alumina as templates for multifunctional applications 2014 *Appl. Phys. Rev.* 1 031102
5. López-Ruiz R, Magén C, Luis F, Bartolomé J, High temperature finite-size effects in the magnetic properties of Ni nanowires 2012, *J. Appl. Phys.* 112, 073906
6. Tomczak P, Ferchmin AR, On the range of interaction from finite size scaling in magnetic Ni nanowires, 2006, *J. Magn. Magn. Mater.* 306, 228.
7. Sousa C T, Leitao D C, Ventura J, Tavares P B and Araujo, J P A versatile synthesis method of dendrites-free segmented nanowires with a precise size control 2012 *Nanoscale Res. Lett.* 7 168
8. Ishrata S, Maaza K, Leeb K J, Jungb M H, Kima G H, Fabrication and temperature-dependent magnetic properties of one-dimensional multilayer Au–Ni–Au–Ni–Au nanowires 2014 *J. Sol. State Chem.* 210 116
9. Maleak N, Potpattanapol P, Bao N N, Ding J, Wongkokuo W, Tang I M, Thongme S., Fabrication and magnetic properties of electrodeposited Ni/Cu nanowires using the double bath method 2014 *J. Mag. Mag. Mater.* 354 262
10. Maleak N, Potpattanapol P, Thongmee S, Bao N N, Ding J and Wongkokuo W, Fabrication and magnetic properties of electrodeposited Ni/Cu nanowires using the double bath method 2014 *J. Mag. Mag. Mater.* 354 262
11. Chen M, Searson P Potential Modulated Multilayer Deposition of Multisegment Cu/Ni Nanowires with Tunable Magnetic Properties 2006 *Chem. Mater.* 18 1595
12. Sun L, Searson P and Chien C Finite-size effects in nickel nanowire arrays 2000 *Phys. Rev. B* 61 6463
13. Beron F, Carignan L P, Menard D and Yelon A, Magnetic Behavior of Ni/Cu Multilayer Nanowire Arrays Studied by First-Order Reversal Curve Diagrams. *Magnetics* 2008 *IEEE Transactions* 44 2745
14. Shakya P, Cox B, and Davis D, Giant Magnetoresistance and Coercivity of electrodeposited multilayered FeCoNi/Cu and CrFeCoNi/Cu 2012 *J. Mag. Mag. Mater.* 324 453
15. Tang X T, Wang G C, and Shima M, Magnetic layer thickness dependence of magnetization reversal in electrodeposited CoNi/Cu multilayer nanowires 2007 *J. Mag. Mag. Mater* 309 188
16. Xu S H, Fei G T, Zhu X G and Zhang L D, Orientation-dependent growth rate of crystalline plane study in electrodeposited Ni/Cu superlattice nanowires 2013 *Cryst. Eng. Comm.* 15 4070
17. Proenca M P, Merazzo K J, Vivas L G, Leitao D C, Sousa C T, Ventura J, Araujo J P and Vazquez M, Co nanostructures in ordered templates: comparative FORC analysis 2013 *Nanotechnol.* 24 475703
18. Vivas L G Vazquez M, Escrig J, Allende S, Altbir D, Leitao D C, and Araujo J P, Magnetic anisotropy in CoNi nanowire arrays: analytical calculations and experiments 2012 *Phys. Rev. B.* 85 035439

19. Leitao D C, Ventura J, Sousa C T, Pereira A M, Sousa J B, Vazquez M, and Araujo J P, Insights into the role of magnetoelastic anisotropy in the magnetization reorientation of magnetic nanowires 2011 *Phys. Rev. B.* 84 014410
20. Sun L, Chien C L, Searson P C, Fabrication of nanoporous single crystal mica templates for electrochemical deposition of nanowire arrays 2000 *J. Mater. Sci.* 35 1097
21. Masuda H and Fukuda K Ordered metal nanohole arrays made by a two-step replication of honeycomb structures of anodic alumina 1995 *Science* 268 1466
22. The OOMMF code is available at <http://math.nist.gov/oommf/>
23. Chen M, Chien CL, Searson PC, Potential Modulated Multilayer Deposition of Multisegment Cu/Ni Nanowires with Tunable Magnetic Properties, 2006 *Chem. Mater.* 18, 1595
24. Guo Y G, Zhu C F, Yang D L, Chen D M and Bai C L Ordered Ni-Cu Nanowire Array with Enhanced Coercivity 2003 *Chem. Mater.* 15 664
25. Ghahremaninezhad A and Dolati A, Diffusion-controlled growth model for electrodeposited cobalt nanowires in highly ordered aluminum oxide membrane 2010 *ECS Transactions* 28 13
26. Graf M, Poppe J, and Eychmuller A, Surface Influences on the Electrodiffusive Behavior in Mesoporous Templates 2015 *Small* 11 3174
27. Proenca M P, Sousa C T, Ventura J, Vazquez M and Araujo JP, Ni growth inside ordered arrays of alumina nanopores: Enhancing the deposition rate 2012 *Electrochim. Acta* 72 215
28. Ji R, Cao C, Chen Z, Yao R, Synthesis of crystalline CoFe_x nanowire arrays through high voltage pulsed electrochemical deposition 2014 *J. Mag. Mag. Mater.* 363 95
29. Nielsch K, Muller F, Lee A P, Gosele U, Uniform Nickel Deposition into Ordered Alumina Pores by Pulsed Electrodeposition 2000 *Adv. Mater.* 12 582
30. Pignard S, Goglio G, Radulescu A, Piraux L, Dubois S, Declémy A and Duvail J L, Study of the magnetization reversal in individual nickel nanowires 2000 *J. Appl. Phys.* 87 824
31. Chen Z, Kunkel H, Zho X, Williams G, Structure and magnetic properties of Fe-Co nanowires in self-assembled arrays 2002 *Phys. Rev. B* 66 134436
32. Aranda P and J M Garcia, Porous membranes for the preparation of magnetic nanostructures 2002 *J. Mag Mag Mater.* 249 214
33. Shi J B, Chen Y C, Lee C W, Lin Y T, Wu C, Chih-Jung Chen, Optical and magnetic properties of 30 and 60 nm Ni nanowires 2008 *Mater. Lett.* 62 15
34. Palmero E M, Real B C, Magen C and Vasquez M, Magnetic behavior of NiCu nanowire arrays: Compositional, geometry and temperature dependence. 2014 *J. Appl. Phys.* 115 114
35. Proenca M P, Sousa C T, Ventura J, and Araujo J P Electrochemical synthesis and magnetism of magnetic nanotubes, in *Magnetic Nano- and Microwires: Design, synthesis, properties and applications* 2015 (Woodhead Publishing, Elsevier) pp 727-781
36. Vazquez M, Hernandez-Velez M, Pirota K, Asenjo A, Navas D, Velazquez J, Vargas P and Ramos C, Arrays of Ni nanowires in alumina membranes: magnetic properties and spatial ordering 2004 *Eur. Phys. J.B* 40 489
37. Sun L, Chien C L, Searson P C, Fabrication of nanoporous single crystal mica templates for electrochemical deposition of nanowire arrays 2000 *J. Mater. Sci.* 35 1097
38. Bergholz R, Gradmann U, Structure and magnetism of oligatomic Ni(111)-films on Re(0001) 1984 *J. Mag. Mag. Mater.* 45 389
39. Huang F, Mankey G J, Kief M T and Willis R F, Finite-size scaling behavior of ferromagnetic thin films 1993 *J. Appl. Phys.* 73 6760
40. Velazquez M, Nielsch K, Vargas P, Velazquez J, Navas D, Pirota K, Hernandez-Velez M, Vogel E, Cartes J, Wehrspohn RB, Gosele U, Modelling hysteresis of interacting nanowires arrays 2004 *Physica B* 343 395

41. Yang CC, Jiang Q, Size and interface effects on critical temperatures of ferromagnetic, ferroelectric and superconductive nanocrystals, 2005, *Acta Materialia* 53, 3305
42. Lu HM, Li PY, Huang YN, Meng XK, Zhang XY, Liu Q, Size-dependent Curie transition of Ni nanocrystals, 2009, *J. Appl. Phys.* 105, 023516
43. Guisbiers G, Buchailot L, Universal size/shape-dependent law for characteristic temperatures, 2009, *Physics Letters A* 374, 305
44. Lang, XY, Zheng WT, Jiang Q, Size and interface effects on ferromagnetic and antiferromagnetic transition temperatures, 2006, *Phys. Rev. B* 73, 224444
45. Velasquez EA, Mazo-Zuluaga J, Mejia-Lopez J, Size dependence study of the ordering temperature in the Fast Monte Carlo method, 2013, *J. Nanopart. Res.* 15, 1437
46. Dalía S B, M B Eduardo and E N Miranda, Analytical solution of the mean field Ising model for finite systems 2012 *J. Phys. Cond. Matter.*, 24 226004
47. Lopez-Dominguez V, Hernandez J M, Tejada J, and Ziolo R F Colossal Reduction in Curie Temperature Due to Finite-Size Effects in CoFe₂O₄ Nanoparticles 2012 *Chem. Mater.* 25 6.

Figures

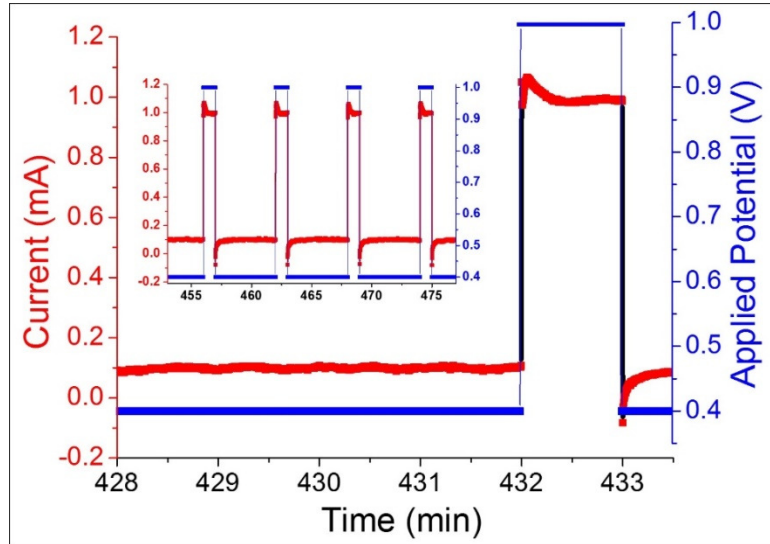


Figure 1 – Selected pulsed electrodeposition potential sequence employed for the synthesis of the multisegmented Ni/Cu NWs in AAO templates, evidencing the Ni deposition pulse of 1 min at -1 V (right), and the respective current during the deposition process (left). Inset shows a sequence of 4 double pulses, illustrating the Ni deposition pulses of 1 min at -1 V, and the Cu deposition pulses of 5 min at -0.4 V.

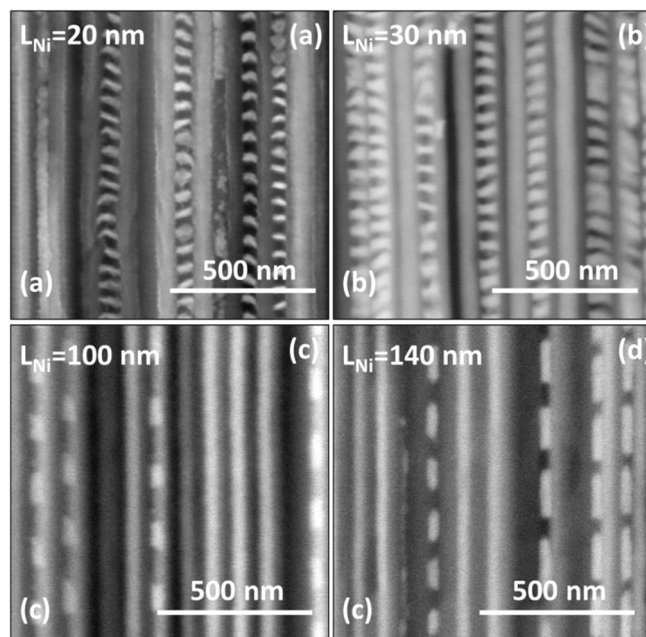


Figure 2 – SEM images of Ni/Cu NWs grown in an AAO template, after partial dissolution of Cu segments, evidencing the Ni segments with lengths (L_{Ni}) of (a) 20 ± 5 nm, (b) 30 ± 7 nm, (c) 100 ± 8 nm and (d) 140 ± 8 nm.

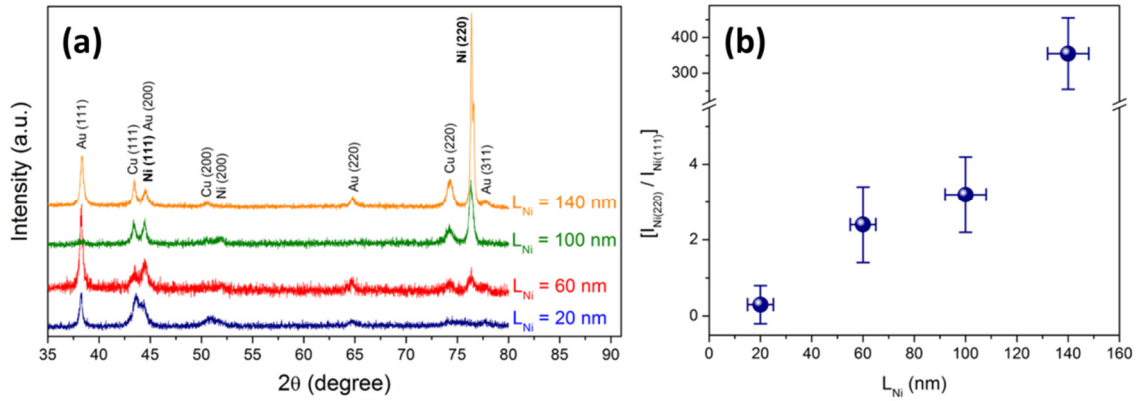


Figure 3 – (a) XRD scans of the multisegmented Ni/Cu NWs with $L_{Ni} = 20 \pm 5$ nm, $L_{Ni} = 60 \pm 5$ nm, $L_{Ni} = 100 \pm 8$ nm and $L_{Ni} = 140 \pm 8$ nm. (b) Ratio between the XRD intensities of the Ni (220) peak and the Ni (111) peak as a function of the L_{Ni} .

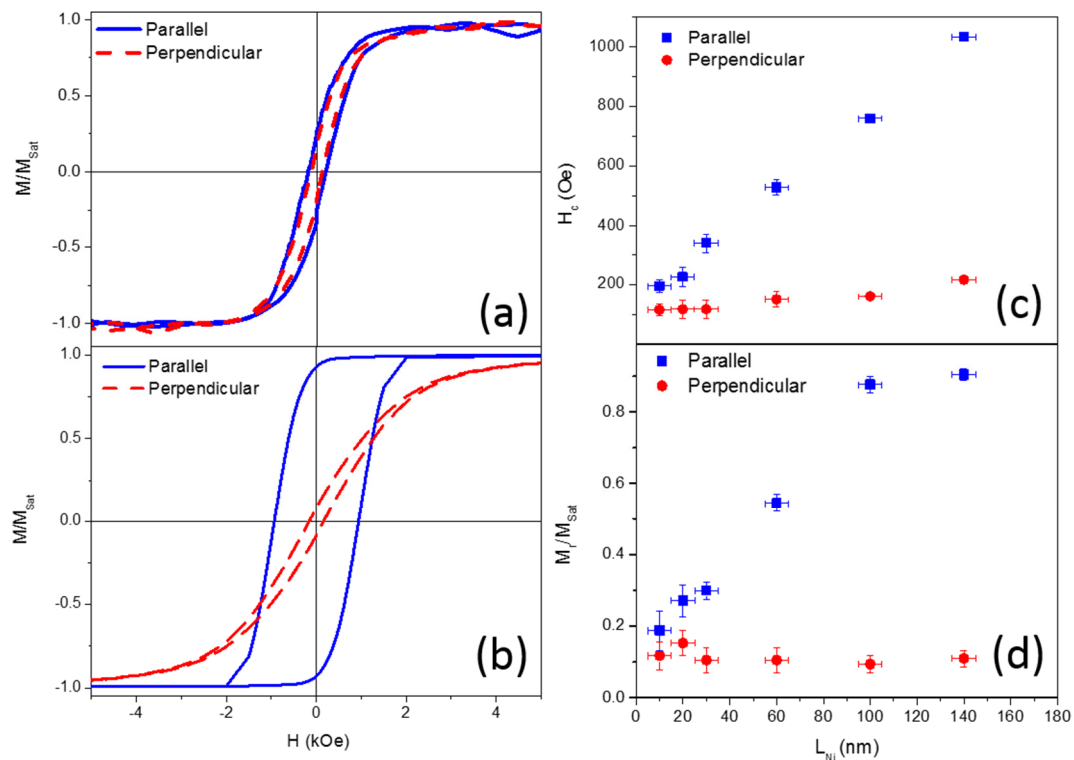


Figure 4 – (a) and (b) magnetic hysteresis loops of ordered arrays of multisegmented Ni/Cu NWs with Ni lengths of (a) 10 ± 5 nm and (b) 100 ± 8 nm, measured along the parallel (blue solid line) and perpendicular (red dashed line) directions. (c) Coercivity (H_c) and (d) normalized

remanence (M_r/M_{Sat}) as a function of the Ni NWs length (L_{Ni}), when applying the magnetic field parallel (blue squares) and perpendicular (red circles) to the NW long axis.

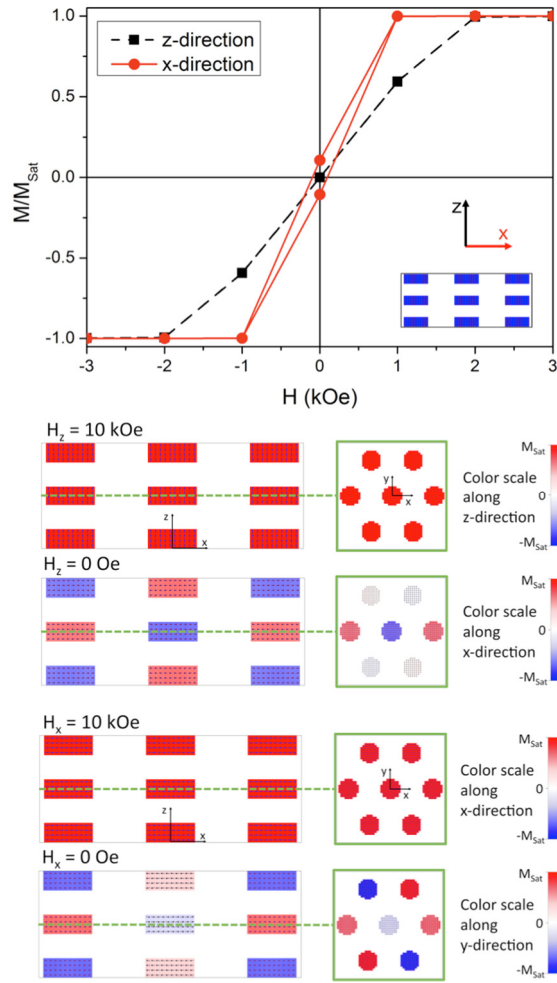


Figure 5 – Simulated magnetic hysteresis loops of a Ni/Cu nanowire array with $L_{Ni} = 20$ nm and $L_{Cu} = 25$ nm, and selected cross-sectional representations (y-slices and z-slices) of the simulated wires, when applying the magnetic field along the z and x directions. Note the different directions of the colour scales.

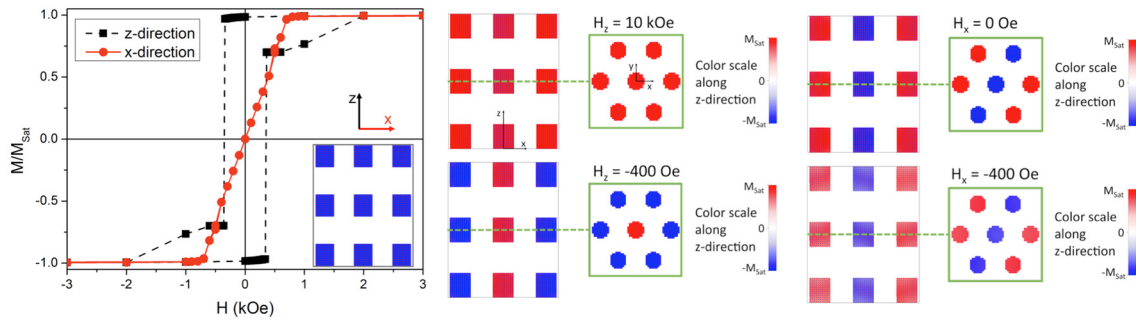


Figure 6 – Simulated magnetic hysteresis loops of a Ni/Cu nanowire array with $L_{Ni} = 60$ nm and $L_{Cu} = 75$ nm, and selected cross-sectional representations (y-slices and z-slices) of the simulated wires, when applying the magnetic field along the z and x directions. Note the different directions of the colour scales.

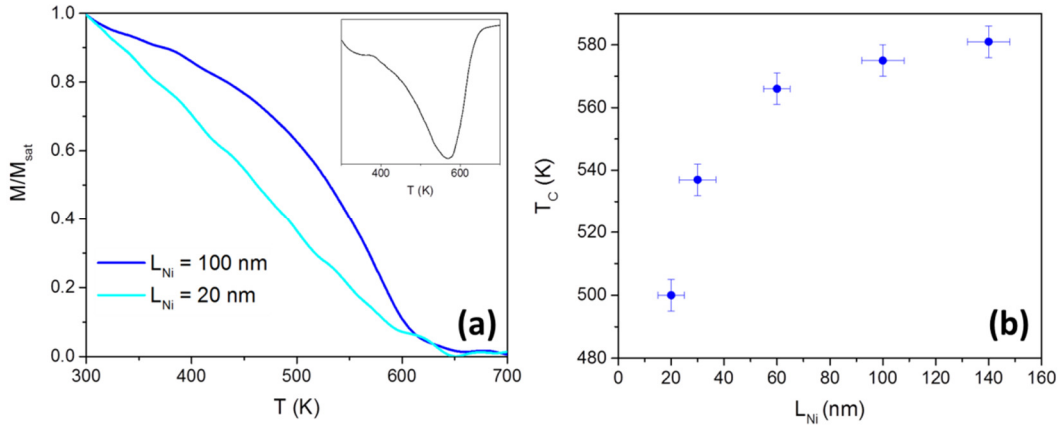


Figure 7 – (a) $M(T)$ measurements obtained for the Ni/Cu NWs with $L_{Ni} = 20$ nm and $L_{Ni} = 100$ nm. Inset shows the derivative of $M(T)$ used to estimate the Curie temperature (T_c) for $L_{Ni} = 100$ nm. (b) Curie temperatures of the produced samples as a function of the L_{Ni} .

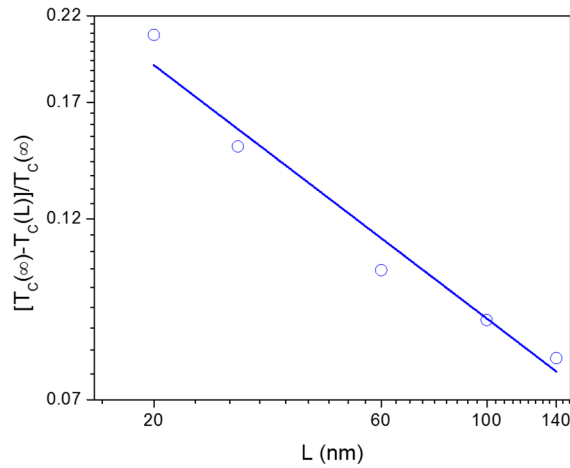


Figure 8 – Log-log plot of the Ni/Cu NWs Curie temperature $[T_c(\infty) - T_c(L)] / T_c(\infty)$ normalized to the Curie temperature for bulk Ni [$T_c(\infty) = 631$ K] versus Ni segment length, L . The solid line corresponds to $\gamma = 0.48$ and $\xi = 8.1$ Å.